FEATURE DRIFT RESILIENT TRACKING OF THE CAROTID ARTERY WALL USING UNSCENTED KALMAN FILTERING WITH DATA FUSION

Jan Dorazil[⋆]*, Rene Repp*[⋆]*, Thomas Kropfreiter*[⋆]*, Richard Prüller*[⋆]*, Kamil Říha*[†]*, and Franz Hlawatsch*[⋆]

[⋆]Institute of Telecommunications, TU Wien, Vienna, Austria (E-mail: doraz.jan@gmail.com)
[†]Department of Telecommunications, Brno University of Technology, Brno, Czech Republic

ABSTRACT

An analysis of the motion of the common carotid artery (CCA) provides effective indicators for cardiovascular diseases. Here, we propose a method for tracking CCA wall motion from a B-mode ultrasound video sequence. An unscented Kalman filter based on a suitably devised state-space model fuses measurements produced by an optical flow algorithm and a CCA wall localization algorithm. This approach compensates for feature drift, which is a detrimental effect in optical flow algorithms. The proposed method is demonstrated to outperform a state-of-the-art tracking method based on optical flow.

***Index Terms*—** Atherosclerosis, common carotid artery, B-mode ultrasound, unscented Kalman filter, data fusion.

1. INTRODUCTION

Atherosclerosis is a major cause of death [1]. Effective indicators for atherosclerosis can be obtained by analyzing the motion of the wall of the common carotid artery (CCA) based on an ultrasound video sequence [2, 3]. Existing methods for estimating CCA wall motion are usually based on speckle tracking [4], which suffers from a detrimental effect known as speckle decorrelation.

One of the first speckle tracking methods for CCA wall motion estimation was based on block matching [5, 6]. The sensitivity to speckle decorrelation was later reduced by using a state-space model for the evolution of the reference block [7, 8] or for the movement of the artery [3, 9]. An alternative to block matching methods is provided by methods based on optical flow [10–14]. A comparison of speckle tracking techniques in [13] showed that a modified Lucas-Kanade optical flow algorithm outperforms other optical flow algorithms as well as block matching algorithms.

In optical flow based methods, speckle decorrelation results in a phenomenon known as feature drift. A CCA wall tracking method that explicitly compensates for feature drift was proposed in [14]. Furthermore, the use of multitarget tracking for CCA wall tracking was recently proposed in [15]. In this approach, distinctive points (so-called feature points) are detected in each ultrasound frame and subsequently tracked across the frames by a Bayesian multitarget tracking algorithm. However, the method is able to provide an accurate estimate only of a relative CCA wall radius displacement, rather than of the absolute radius. All the mentioned methods analyze longitudinal scans of the CCA, with the exception of [11, 14, 15], which analyze transverse scans.

In this work, we propose an optical flow based CCA wall tracking method that uses a Bayesian tracking approach combined with data fusion to achieve resilience to feature drift. Following [11, 14, 15], our method processes B-mode ultrasound sequences of arbitrary length that show the CCA transverse section. Based on a new state-space model for CCA wall motion, we employ the unscented Kalman filter (UKF) [16] to track the time-varying center point and radius of a circle describing the CCA wall cross section. The UKF fuses measurements provided by the pyramidal Lucas-Kanade optical flow algorithm [17] and by a circle localization algorithm [18]. This data fusion approach results in an inherent compensation of feature drift that strongly improves on the feature drift compensation performed in [14] in that it operates in a temporally consistent manner that takes into account the natural smoothness of CCA wall motion. Our method also improves on the multitarget tracking method of [15] in that it provides highly accurate absolute CCA wall radius estimates, rather than just relative displacement estimates. We note that the application of a UKF to CCA wall motion tracking has been proposed previously in [3], however for analyzing longitudinal (rather than transverse) CCA scans, based on a different state-space model, and not using our data fusion approach.

This paper is organized as follows. Section 2 gives an overview of the proposed method. The state-space model underlying our method is described in Section 3. In Section 4, the operation of the UKF is discussed. Simulation results are presented in Section 5.

2. METHOD OVERVIEW

The proposed fusion-and-tracking method combines the pyramidal Lucas-Kanade optical flow algorithm of [17], the circle localization algorithm of [18], and the UKF in a frame-sequential, frame-recursive manner. The optical flow algorithm performs a first, crude tracking of a set of *feature points* (FPs) around the CCA wall. Here, an FP is a point in the ultrasound frame that corresponds to a high response of the Harris detector [19] and can thus be assumed to represent the local tissue movement. The input to our method is a B-mode ultrasound video sequence whose frames $\boldsymbol{I}_t$ show temporally successive transverse scans of the CCA. Fig. 1 visualizes the main steps of our method that are performed during one recursion corresponding to frame (or time) index t. Fig. 2 depicts the CCA wall representation by a circle (hereafter briefly termed "CCA circle") and some surrounding FPs. We denote the center point of the CCA circle by $\boldsymbol{c}_t$, the circle radius by r_t, the two-dimensional position of the n-th FP by $\boldsymbol{y}_t^{(n)}$, the FP's distance from $\boldsymbol{c}_t$ (briefly termed "FP radius") by $\rho_t^{(n)}$, and the FP's angle relative to $\boldsymbol{c}_t$ by $\theta_t^{(n)}$.

For each frame $\boldsymbol{I}_t$, $t = 1, 2, \ldots$, the proposed method calculates a list $\hat{\boldsymbol{Y}}_t$ of N_t FP position estimates $\hat{\boldsymbol{y}}_t^{(n)}$, $n = 1, 2, \ldots, N_t$ as well as estimates $\hat{\boldsymbol{c}}_t$ and $\hat{r}_t$ of the center point and radius of the CCA circle. For the first frame, $t = 1$, the FP position list $\hat{\boldsymbol{Y}}_1$ is empty and the CCA circle parameter estimates $\hat{\boldsymbol{c}}_1$ and $\hat{r}_1$ are obtained by applying the circle localization algorithm of [18] to $\boldsymbol{I}_1$. For the further frames $t = 2, 3, \ldots$, the quantities $\hat{\boldsymbol{Y}}_t$, $\hat{\boldsymbol{c}}_t$, and $\hat{r}_t$ are calculated frame-sequentially by performing the following steps (cf. Fig. 1).

This work was supported by the Czech Science Foundation (GAČR) under grant 17-19638S and by the Czech Ministry of Education, Youth and Sports under grant 8J19AT029.

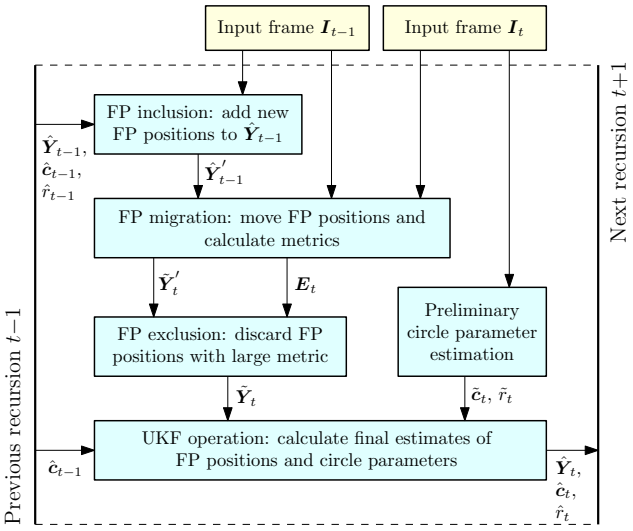

Fig. 1. Main steps of the proposed method for frame t.

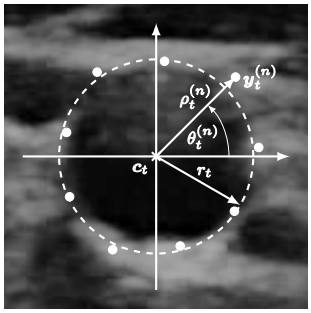

Fig. 2. CCA circle and surrounding FPs.

FP inclusion: First, we update the previous FP position list $\hat{\boldsymbol{Y}}_{t-1}$. Using the Harris detector [19], we detect a list $\boldsymbol{Y}_t^{\text{new}}$ of new potential FPs inside an annular region of the previous frame $\boldsymbol{I}_{t-1}$ with center $\hat{\boldsymbol{c}}_{t-1}$ and inner/outer radii $\hat{r}_{t-1} \pm \Delta_r$, with some $\Delta_r > 0$. The updated list $\hat{\boldsymbol{Y}}'_{t-1}$ includes all FP positions from $\hat{\boldsymbol{Y}}_{t-1}$ plus some FP positions from $\boldsymbol{Y}_t^{\text{new}}$. These latter FPs are selected such that they have a high Harris response [19] and the distance between any two FPs in $\hat{\boldsymbol{Y}}'_{t-1}$ is larger than a threshold $d>0$.

FP migration: Next, we use the pyramidal Lucas-Kanade optical flow algorithm [17] to move each FP position $\hat{\boldsymbol{y}}_{t-1}^{(n)\prime}$ in $\hat{\boldsymbol{Y}}'_{t-1}$ to a new position $\tilde{\boldsymbol{y}}_t^{(n)\prime}$ that takes into account the current frame $\boldsymbol{I}_t$. This results in a new FP position list $\tilde{\boldsymbol{Y}}'_t$. For each new position $\tilde{\boldsymbol{y}}_t^{(n)\prime}$, we calculate a metric $\varepsilon_t^{(n)}$ as the sum of absolute differences between the pixel intensities of an $m\times m$ patch of $\boldsymbol{I}_{t-1}$ centered at $\hat{\boldsymbol{y}}_{t-1}^{(n)\prime}$ and those of an $m\times m$ patch of $\boldsymbol{I}_t$ centered at $\tilde{\boldsymbol{y}}_t^{(n)\prime}$. The resulting list of metrics, denoted by $\boldsymbol{E}_t$, accompanies the FP position list $\tilde{\boldsymbol{Y}}'_t$.

FP exclusion: FPs that satisfy $\varepsilon_t^{(n)} > \alpha\bar{\varepsilon}_t$, where $\bar{\varepsilon}_t$ is the average of all metrics in $\boldsymbol{E}_t$ and $\alpha > 1$ is a fixed parameter, are considered to be outliers and are thus excluded from the FP position list $\tilde{\boldsymbol{Y}}'_t$. The FPs surviving this exclusion step form a "preliminary" FP position list $\tilde{\boldsymbol{Y}}_t$ containing N_t FP positions $\tilde{\boldsymbol{y}}_t^{(n)}$, $n = 1, 2, \ldots, N_t$. (Note that N_t, the time-dependent number of FPs, is determined by the FP inclusion and exclusion steps.) The FP position list $\tilde{\boldsymbol{Y}}_t$ constitutes one of the two inputs to the UKF.

Preliminary circle parameter estimation: The other UKF input is obtained by applying the circle localization algorithm of [18] to the current frame $\boldsymbol{I}_t$. This results in "preliminary" circle parameter estimates $\tilde{\boldsymbol{c}}_t$ and $\tilde{r}_t$.

UKF operation: The UKF operates on the preliminary FP position list $\tilde{\boldsymbol{Y}}_t$ and the preliminary circle parameter estimates $\tilde{\boldsymbol{c}}_t$ and $\tilde{r}_t$, which serve as "observed measurements." The UKF fuses these measurements to recursively calculate final FP position estimates $\hat{\boldsymbol{y}}_t^{(n)}$, $n = 1, 2, \ldots, N_t$, which constitute the final FP position list $\hat{\boldsymbol{Y}}_t$, as well as final circle parameter estimates $\hat{\boldsymbol{c}}_t$ and $\hat{r}_t$. This is described in Section 4. The sequence of radius estimates $\hat{r}_t$ for $t = 1, 2, \ldots$ is the overall output of our method. The operation of the UKF is based on a probabilistic state-space model, which will be developed next.

3. SYSTEM MODEL

A main contribution of our work is the establishment of a state-space model that describes the dynamics of CCA wall motion (state evolution model) and a related measurement process (measurement model). The proposed model is partly inspired by [20]. The measurement model underlies the fusion performed by the UKF.

3.1. CCA Circle Radius, FP Radii, State Vector

The heartbeat manifests itself in an approximately periodic movement of the CCA wall. This suggests the use of a Fourier series with slowly time-varying Fourier coefficients to model the CCA wall movement [21, Ch. 11]. More specifically, we model the time-dependent CCA circle radius r_t as

$$r_t = R + \sum_{m=1}^{M} \left(a_t^{(m)} \cos(m\omega t) + b_t^{(m)} \sin(m\omega t) \right) + \gamma_t, \qquad (1)$$

where the constant R is the mean CCA circle radius, $a_t^{(m)}$ and $b_t^{(m)}$ are time-varying Fourier coefficients, γ_t represents the effect of breathing [22], and ω is the fundamental frequency (which is assumed to be known; however, our tracking framework can be extended to include tracking of ω). Using r_t, we can express the n-th FP radius with respect to the CCA circle center $\boldsymbol{c}_t$ (see Fig. 2) as

$$\rho_t^{(n)} = r_t + \tilde{\delta}^{(n)} + \delta_t^{(n)}, \quad n = 1, 2, \ldots, N_t, \qquad (2)$$

where $\tilde{\delta}^{(n)}$ denotes an initial approximation of the radial deviation of the FP from the CCA circle, $\delta_t^{(n)}$ denotes a time-dependent radial deviation, and N_t is the number of FP positions tracked at frame time t by the UKF.

We now define the *system state* to be the $2M+2N_t+4$ dimensional vector

$$\boldsymbol{x}_t \triangleq \left(\boldsymbol{a}_t^{\mathrm{T}} \; \boldsymbol{b}_t^{\mathrm{T}} \; \gamma_t \; R_t \; \boldsymbol{c}_t^{\mathrm{T}} \; \boldsymbol{p}_t^{(1)\mathrm{T}} \; \boldsymbol{p}_t^{(2)\mathrm{T}} \cdots \boldsymbol{p}_t^{(N_t)\mathrm{T}} \right)^{\mathrm{T}}, \qquad (3)$$

where $\boldsymbol{a}_t \triangleq (a_t^{(1)} \cdots a_t^{(M)})^{\mathrm{T}}$, $\boldsymbol{b}_t \triangleq (b_t^{(1)} \cdots b_t^{(M)})^{\mathrm{T}}$, R_t is a (formally) time-dependent version of the mean CCA circle radius R in (1), and $\boldsymbol{p}_t^{(n)} \triangleq (\delta_t^{(n)} \; \theta_t^{(n)})^{\mathrm{T}}$ (referred to as FP position parameter vector). Note that from the state $\boldsymbol{x}_t$, one can obtain the CCA circle center $\boldsymbol{c}_t$ (which is a subvector of $\boldsymbol{x}_t$), the CCA circle radius r_t (via (1)), and all the FP positions up to the initial radial deviation approximations $\tilde{\delta}^{(n)}$ (from the subvectors $\boldsymbol{p}_t^{(n)}$, using (2) and (1)).

3.2. State Evolution Model

For a basic formulation of the state evolution model underlying the UKF, we temporarily assume that the number of FPs $N_t = N$ and

consequently the state dimension $2M+2N+4=L$ are constant; an extension to time-dependent N and L will be given in Section 4.1. We use the linear state evolution model given by

$$\boldsymbol{x}_t = \boldsymbol{\Phi}\boldsymbol{x}_{t-1} + \boldsymbol{u}_t, \quad t = 1, 2, \ldots.$$

Here, $\boldsymbol{\Phi}$ is an $L \times L$ diagonal matrix defined as (cf. (3))

$$\boldsymbol{\Phi} \triangleq \operatorname{diag}\{\underbrace{1, \ldots, 1}_{2M \text{ times "1"}}, \phi_\gamma, 1, 1, 1, \underbrace{\phi_\delta, 1, \ldots, \phi_\delta, 1}_{N \text{ times "}\phi_\delta\text{, 1"}}\}, \tag{4}$$

with $\phi_\gamma, \phi_\delta \in [0, 1]$. Furthermore, $\boldsymbol{u}_t$ is an L-dimensional driving process that is independent and identically distributed (iid) and zero-mean with covariance matrix

$$\boldsymbol{C}_u \triangleq \operatorname{diag}\{\underbrace{\sigma_{ab}^2, \ldots, \sigma_{ab}^2}_{2M \text{ times "}\sigma_{ab}^2\text{"}}, \sigma_\gamma^2, 0, \sigma_c^2, \sigma_c^2, \underbrace{\sigma_\delta^2, \sigma_\theta^2, \ldots, \sigma_\delta^2, \sigma_\theta^2}_{N \text{ times "}\sigma_\delta^2, \sigma_\theta^2\text{"}}\}. \tag{5}$$

Accordingly, the state evolution models for $a_t^{(m)}$ and $b_t^{(m)}$ ($m = 1, 2, \ldots, M$) as well as for $c_t^{(1)}$, $c_t^{(2)}$, and $\theta_t^{(n)}$ ($n = 1, 2, \ldots, N$) are random walk models, the state evolution models for γ_t and $\delta_t^{(n)}$ are first-order autoregressive models, and R_t is modeled as constant (because the corresponding driving noise variance is zero).

3.3. Measurement Model

According to Section 2, the "measurements" constituting the input to the UKF are the preliminary FP positions $\tilde{\boldsymbol{y}}_t^{(n)}$, $n = 1, 2, \ldots, N$ and the preliminary circle parameter estimates $\tilde{\boldsymbol{c}}_t$ and $\tilde{r}_t$. Thus, the overall measurement vector at frame time t is given by $\boldsymbol{z}_t \triangleq \big(\tilde{\boldsymbol{y}}_t^{(1)\mathrm{T}}\ \tilde{\boldsymbol{y}}_t^{(2)\mathrm{T}} \cdots \tilde{\boldsymbol{y}}_t^{(N)\mathrm{T}}\ \tilde{\boldsymbol{c}}_t^{\mathrm{T}}\ \tilde{r}_t\big)^{\mathrm{T}}$. The measurement model underlying the UKF relates these measurements to the state vector $\boldsymbol{x}_t$ in a probabilistic manner.

We model the preliminary FP position estimates $\tilde{\boldsymbol{y}}_t^{(n)}$ as

$$\tilde{\boldsymbol{y}}_t^{(n)} = \boldsymbol{g}(\rho_t^{(n)}, \theta_t^{(n)}) + \boldsymbol{c}_t + \boldsymbol{v}_t^{(n)}, \quad n = 1, 2, \ldots, N. \tag{6}$$

Here, $(\rho_t^{(n)}, \theta_t^{(n)})$ is the true FP position, relative to the CCA circle center $\boldsymbol{c}_t$, expressed in polar coordinates; the function $\boldsymbol{g}(\cdot, \cdot)$ maps polar coordinates to Cartesian coordinates; and the measurement noise processes $\boldsymbol{v}_t^{(n)}$ are mutually independent, iid, zero-mean, two-dimensional processes with covariance matrix $\boldsymbol{C}_{v^{(n)}} \triangleq \operatorname{diag}\{\sigma_{v,1}^2, \sigma_{v,2}^2\}$. Recalling that $\rho_t^{(n)}$ is given by (2) and (1) with R formally replaced by R_t, it is seen that expression (6) involves the state components (cf. (3)) $\boldsymbol{a}_t$, $\boldsymbol{b}_t$, γ_t, R_t, $\boldsymbol{c}_t$, and $\boldsymbol{p}_t^{(n)} = (\delta_t^{(n)}\ \theta_t^{(n)})^{\mathrm{T}}$ for $n = 1, 2, \ldots, N$. Furthermore, we model the preliminary circle parameter estimates $\tilde{\boldsymbol{c}}_t$ and $\tilde{r}_t$ as

$$\tilde{\boldsymbol{c}}_t = \boldsymbol{c}_t + \boldsymbol{v}_t^{(\mathrm{c})}, \quad \tilde{r}_t = r_t + v_t^{(\mathrm{r})}, \tag{7}$$

where $\boldsymbol{v}_t^{(\mathrm{c})}$ and $v_t^{(\mathrm{r})}$ are iid zero-mean measurement noise processes with covariance $\boldsymbol{C}_{v^{(\mathrm{c})}} \triangleq \sigma_{v^{(\mathrm{c})}}^2 \mathbf{I}_2$ and variance $\sigma_{v^{(\mathrm{r})}}^2$, respectively. The expressions (7) involve the state components $\boldsymbol{a}_t$, $\boldsymbol{b}_t$, γ_t, R_t, and $\boldsymbol{c}_t$.

4. UKF OPERATION

Let $\boldsymbol{z}_{1:t} \triangleq (\boldsymbol{z}_1^{\mathrm{T}} \cdots \boldsymbol{z}_t^{\mathrm{T}})^{\mathrm{T}}$ be the vector stacking all the measurements up to the current frame time t. We employ the UKF [16] to recursively calculate estimates of the posterior mean and covariance of the state $\boldsymbol{x}_t$ given $\boldsymbol{z}_{1:t}$, i.e., $\hat{\boldsymbol{x}}_t \approx \mathrm{E}\{\boldsymbol{x}_t | \boldsymbol{z}_{1:t}\}$ and $\boldsymbol{P}_t \approx \mathrm{Cov}\{\boldsymbol{x}_t | \boldsymbol{z}_{1:t}\}$. From $\hat{\boldsymbol{x}}_t$, we can in turn obtain estimates of the FP positions $\boldsymbol{y}_t^{(n)}$, $n = 1, 2, \ldots, N$ as well as of the CCA circle center point $\boldsymbol{c}_t$ and the CCA circle radius r_t via (1)–(3). We adopt the UKF, rather than simply the Kalman filter [23, Ch. 2], because our measurement model (6) is nonlinear (due to $\boldsymbol{g}(\cdot, \cdot)$). Moreover, compared to the extended Kalman filter [23, Ch. 2], the UKF usually provides a better performance at a similar computational complexity [16].

We use a slight modification of the UKF algorithm of [16] that accounts for the time-varying number $L_t = 2M + 2N_t + 4$ of state components. In the rest of this section, we will focus on this modification since a detailed discussion of the basic UKF algorithm can be found in [16].

4.1. FP Allocation/Deallocation

In the FP inclusion step described in Section 2, new FP positions are added to the previous FP position list $\hat{\boldsymbol{Y}}_{t-1}$. According to (3), the inclusion of a new FP n in $\hat{\boldsymbol{Y}}_{t-1}$ entails a corresponding allocation (insertion) of the FP position parameter vector $\boldsymbol{p}_{t-1}^{(n)}$ in the state vector $\boldsymbol{x}_{t-1}$, which in turn implies an analogous allocation of an estimate of $\boldsymbol{p}_{t'}^{(n)}$ in the state estimate vector $\hat{\boldsymbol{x}}_{t'}$ for $t' = t-1, t, \ldots$. This estimate is initialized as $\hat{\boldsymbol{p}}_{t-1}^{(n)} \triangleq (\hat{\delta}_{t-1}^{(n)}\ \hat{\theta}_{t-1}^{(n)})^{\mathrm{T}} = \big(0\ \ \tan^{-1}(\xi_{t-1}^{(2)}/\xi_{t-1}^{(1)})\big)^{\mathrm{T}}$. Here, $\xi_{t-1}^{(1)}$ and $\xi_{t-1}^{(2)}$ are the Cartesian coordinates of $\boldsymbol{\xi}_{t-1} \triangleq \hat{\boldsymbol{y}}_{t-1}^{(n)\prime} - \hat{\boldsymbol{c}}_{t-1}$, in which $\hat{\boldsymbol{y}}_{t-1}^{(n)\prime} \in \hat{\boldsymbol{Y}}_{t-1}^{\prime}$ is the FP position estimate obtained in the FP inclusion step (see Section 2) and $\hat{\boldsymbol{c}}_{t-1}$ is the previous estimate of the circle center. Furthermore, associated variances are allocated as two additional elements on the diagonal of the covariance matrix estimate $\boldsymbol{P}_{t'}$ for $t' = t-1, t, \ldots$. These variances are initialized in $\boldsymbol{P}_{t-1}$ as s_δ^2 and s_θ^2, which express our a priori uncertainty about $\delta_{t-1}^{(n)}$ and $\theta_{t-1}^{(n)}$, respectively. In addition, an initial approximation of the radial deviation of the new FP from the previous CCA circle estimate is calculated as $\tilde{\delta}^{(n)} = \|\boldsymbol{\xi}_{t-1}\| - \hat{r}_{t-1}$. Note that $\tilde{\delta}^{(n)}$ is not part of the state vector $\boldsymbol{x}_t$ but it is used in the FP radius model (2) for $t' = t-1, t, \ldots$.

Similar allocation operations are carried out for the matrices $\boldsymbol{\Phi}$ in (4) and $\boldsymbol{C}_u$ in (5), which thereby become time-dependent. More specifically, for $t' = t-1, t, \ldots$, ϕ_δ and 1 are inserted as additional diagonal elements of $\boldsymbol{\Phi}_{t'}$, and σ_δ^2 and σ_θ^2 are inserted as additional diagonal elements of $\boldsymbol{C}_{u,t'}$.

Conversely, in the FP exclusion step described in Section 2, some of the FPs are excluded from the FP position list $\tilde{\boldsymbol{Y}}_t^{\prime}$. The exclusion of FP n at time t entails a deallocation (removal) of $\boldsymbol{p}_{t-1}^{(n)}$ in the state vector $\boldsymbol{x}_{t-1}$. This implies analogous deallocation operations in $\hat{\boldsymbol{x}}_{t'}$, $\boldsymbol{P}_{t'}$, $\boldsymbol{\Phi}_{t'}$, and $\boldsymbol{C}_{u,t'}$ for $t' = t-1, t, \ldots$.

4.2. Initialization

The recursive UKF algorithm is initialized at frame time $t = 1$ as follows. Since no FPs are allocated yet, i.e., $N_1 = 0$, we choose the mean $\hat{\boldsymbol{x}}_1$ and covariance matrix $\boldsymbol{P}_1$ as (cf. (3))

$$\hat{\boldsymbol{x}}_1 = (\underbrace{0\ \ 0 \cdots 0}_{2M+1 \text{ times "0"}}\ \hat{r}_1\ \hat{\boldsymbol{c}}_1^{\mathrm{T}})^{\mathrm{T}},$$

$$\boldsymbol{P}_1 = \operatorname{diag}\{\underbrace{s_{ab}^2, s_{ab}^2, \ldots, s_{ab}^2}_{2M \text{ times "}s_{ab}^2\text{"}}, s_\gamma^2, s_R^2, s_c^2, s_c^2\}.$$

Here, $\hat{r}_1$ and $\hat{\boldsymbol{c}}_1$ are obtained from the circle localization algorithm of [18], and the variances s_{ab}^2, s_γ^2, s_R^2, and s_c^2 express our a priori uncertainty about the $a_1^{(m)}$ and $b_1^{(m)}$ ($m = 1, 2, \ldots, M$) and about γ_1, R_1, and $c_1^{(1)}$ and $c_1^{(2)}$, respectively.

5. SIMULATION RESULTS

To demonstrate the performance of our method, we applied it to two different datasets of synthetic CCA ultrasound sequences. The first

Sequence	RMSE		SD	
	Proposed method	Reference method	Proposed method	Reference method
S_{∞}	49.42	89.30	—	—
S_{25}^{+}	31.66	71.54	1.06	31.01
S_{15}^{+}	28.58	119.96	3.09	51.96
S_{25}^{*}	39.44	155.74	6.56	110.47
S_{15}^{*}	29.18	140.18	3.03	84.49

Table 1. RMSE and SD (both in μm) for dataset S.

dataset, labeled S, consists of five sequences dubbed S_{∞}, S_{25}^{+}, S_{15}^{+}, S_{25}^{*}, and S_{15}^{*}. These sequences were created by performing a time-varying deformation of a real ultrasound image according to the mathematical model of radial CCA wall motion presented in [24], and including additive or multiplicative Gaussian noise. The subscripts ∞, 25, and 15 indicate the signal-to-noise ratio in decibels, and the superscripts $+$ and $*$ indicate the nature of the noise (additive or multiplicative). Each sequence consists of T=1324 ultrasound frames. For each of the noisy sequences S_{25}^{+}, S_{15}^{+}, S_{25}^{*}, and S_{15}^{*}, we generated K=100 realizations that differed in the noise realization.

The second dataset, labeled F, consists of the sequences F_0, F_2, and F_5. Sequence F_0 was created using the Field II ultrasound simulation program [25]. The first frame ($t = 1$) was obtained by randomly generating a set of 10^5 scatterers distributed uniformly on the image region. The amplitudes of the scatterers were determined by an echogenicity map that was created by smoothing and posterizing a real ultrasound image. For each subsequent frame $t = 2, 3, \ldots, T$=1324 of F_0, we generated a new set of scatterers by displacing the initial scatterers according to the mathematical model of CCA wall movement in [24]. The sequences F_2 and F_5 were then derived from F_0 via a modification simulating speckle decorrelation. In each frame t of F_0, a specified proportion of scatterers was replaced by new scatterers that were randomly (uniformly) drawn in the image region. The subscripts 2 and 5 indicate the proportion of replaced scatterers in percent. For these sequences, we generated only one realization because of the high runtime of the Field II simulations. A more detailed description of the generation of the S and F sequences can be found in [14].

We compare our method with the state-of-the-art method recently presented in [14], which will be referred to as "reference method." This method also uses the pyramidal Lucas-Kanade optical flow algorithm [17] but combats feature drift by replacing FPs that drifted too far from the current CCA circle estimate with new FPs (instead of using the proposed fusion-and-tracking approach based on the UKF and the circle localization algorithm of [18]). We note that we do not include a comparison with the multitarget tracking method of [15] because that method is able to provide accurate estimates only of relative CCA wall radius displacements.

We assess the performance of our method and the reference method by the empirical root-mean-square error (RMSE) defined as RMSE $\triangleq \left(\frac{1}{K}\sum_{k=1}^{K} e_k^2\right)^{1/2}$ with $e_k \triangleq \left(\frac{1}{T}\sum_{t=1}^{T}(\hat{r}_{t,k} - r_t)^2\right)^{1/2}$ (here, k is the realization index, $\hat{r}_{t,k}$ denotes the CCA radius estimate obtained for realization k, and r_t denotes the true CCA radius). In addition, for the noisy sequences S_{25}^{+}, S_{15}^{+}, S_{25}^{*}, and S_{15}^{*} (for which $K = 100$), we also consider the inter-realization empirical standard deviation of e_k defined as SD $\triangleq \left(\frac{1}{K}\sum_{k=1}^{K}(e_k - \bar{e}_k)^2\right)^{1/2}$ with $\bar{e}_k \triangleq \frac{1}{K}\sum_{k=1}^{K} e_k$. Note that SD is not meaningful for S_{∞}, F_0, F_2, and F_5, since for these sequences K=1. The results we obtained for datasets S and F are listed in Tables 1 and 2, respectively. It can be observed that the RMSE of the proposed method is always significantly smaller than that of the reference method. Moreover, the SD results indicate that the performance of the proposed method is significantly more consistent over multiple simulation runs.

Sequence	Proposed method	Reference method
F_0	21.14	64.92
F_2	26.60	178.16
F_5	17.50	77.50

Table 2. RMSE (in μm) for dataset F.

Fig. 3 shows the estimated radius sequence $\hat{r}_{t,1}$ (note that $k = 1$) that we obtained with the proposed method and with the reference method for sequence F_2, along with the true radius sequence and the absolute estimation error. These results confirm that the estimation accuracy of the proposed method is significantly better than that of the reference method.

6. CONCLUSION

We proposed a method for tracking a circular approximation of the cross section of the common carotid artery (CCA) wall, given a B-mode ultrasound video sequence of arbitrary length. Our method features two successive tracking stages, the first using an optical flow algorithm and the second using an unscented Kalman filter (UKF). The UKF stage allows an inherent compensation of the detrimental feature drift effect limiting the performance of optical flow algorithms. This compensation is achieved by fusing the results of the optical flow algorithm with preliminary circle estimates produced by a circle localization method. The operation of the UKF relies on a new state-space model that describes the dynamics of CCA wall motion and a related measurement process. A numerical evaluation of our method for synthetic datasets emulating speckle decorrelation as well as additive and multiplicative noise demonstrated significant performance advantages over a state-of-the-art method [14].

Interesting directions of future research include the integration of the fundamental frequency ω, and possibly of other system parameters, into the state vector; the consideration of more detailed contours characterizing the CCA wall cross section; the use of an improved optical flow algorithm (e.g., based on an affine model for the velocity field [26]); and the estimation of clinically relevant parameters such as radial and longitudinal strain [21].

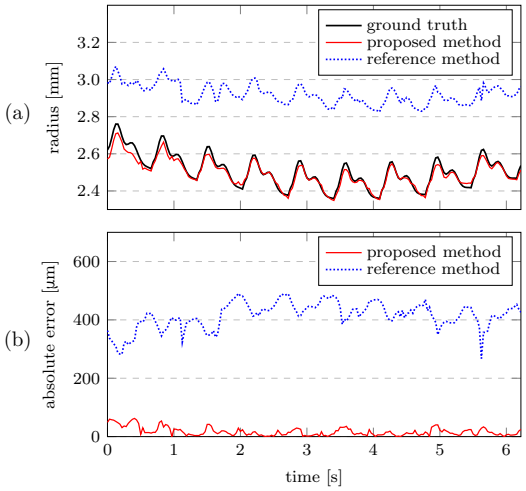

Fig. 3. Estimation results for sequence F_2 during the first 200 frames: (a) Radius estimates and true radius, (b) absolute estimation errors.

7. REFERENCES

[1] World Health Organization, "World Health Statistics 2018: Monitoring health for the SDGs, sustainable development goals," Geneva, Switzerland, 2018.

[2] M. Mokhtari-Dizaji, M. Montazeri, and H. Saberi, "Differentiation of mild and severe stenosis with motion estimation in ultrasound images," *Ultrasound Med. Biol.*, vol. 32, no. 10, pp. 1493–1498, Oct. 2006.

[3] Z. Gao, Y. Li, Y. Sun, J. Yang, H. Xiong, H. Zhang, X. Liu, W. Wu, D. Liang, and S. Li, "Motion tracking of the carotid artery wall from ultrasound image sequences: A nonlinear state-space approach," *IEEE Trans. Med. Imaging*, vol. 37, no. 1, pp. 273–283, Jan. 2017.

[4] E. J. Chen, R. S. Adler, P. L. Carson, W. K. Jenkins, and W. D. O'Brien, "Ultrasound tissue displacement imaging with application to breast cancer," *Ultrasound Med. Biol.*, vol. 21, no. 9, pp. 1153–1162, Jan. 1995.

[5] S. Golemati, A. Sassano, M. J. Lever, A. A. Bharath, S. Dhanjil, and A. N. Nicolaides, "Carotid artery wall motion estimated from B-mode ultrasound using region tracking and block matching," *Ultrasound Med. Biol.*, vol. 29, no. 3, pp. 387–399, Mar. 2003.

[6] J. Tat, J. S. Au, P. J. Keir, and M. J. MacDonald, "Reduced common carotid artery longitudinal wall motion and intramural shear strain in individuals with elevated cardiovascular disease risk using speckle tracking," *Clin. Physiol. Funct. Imag.*, vol. 37, no. 2, pp. 106–116, Mar. 2017.

[7] A. Gastounioti, S. Golemati, J. Stoitsis, and K. S. Nikita, "Kalman-filter-based block matching for arterial wall motion estimation from B-mode ultrasound," in *Proc. IEEE Int. Conf. Imaging Syst. Tech.*, Thessaloniki, Greece, Jul. 2010, pp. 234–239.

[8] G. Zahnd, M. Orkisz, A. Sérusclat, P. Moulin, and D. Vray, "Evaluation of a Kalman-based block matching method to assess the bi-dimensional motion of the carotid artery wall in B-mode ultrasound sequences," *Med. Image Anal.*, vol. 17, no. 5, pp. 573–585, Jul. 2013.

[9] A. Gastounioti, S. Golemati, J. Stoitsis, and K. Nikita, "Comparison of Kalman-filter-based approaches for block matching in arterial wall motion analysis from B-mode ultrasound," *Meas. Sci. Technol.*, vol. 22, no. 11, pp. 1–9, Oct. 2011.

[10] B. D. Lucas and T. Kanade, "An iterative image registration technique with an application to stereo vision," in *Proc. Int. Joint Conf. Artif. Intell.*, Vancouver, BC, Canada, Aug. 1981, pp. 674–679.

[11] K. Říha and I. Potůček, "The sequential detection of artery sectional area using optical flow technique," in *Proc. WSEAS Int. Conf. Circ. Syst. Electron. Contr. Signal Process.*, Stevens Point, WI, USA, Dec. 2009, pp. 222–226.

[12] A. Gastounioti, N. N. Tsiaparas, S. Golemati, J. S. Stoitsis, and K. S. Nikita, "Affine optical flow combined with multiscale image analysis for motion estimation of the arterial wall from B-mode ultrasound," in *Proc. Ann. Int. Conf. IEEE Eng. Med. Biol. Soc.*, Boston, MA, USA, Aug. 2011, pp. 559–562.

[13] S. Golemati, J. S. Stoitsis, A. Gastounioti, A. C. Dimopoulos, V. Koropouli, and K. S. Nikita, "Comparison of block matching and differential methods for motion analysis of the carotid artery wall from ultrasound images," *IEEE Trans. Inf. Technol. Biomed.*, vol. 16, no. 5, pp. 852–858, Sep. 2012.

[14] K. Říha, M. Zukal, and F. Hlawatsch, "Analysis of carotid artery transverse sections in long ultrasound video sequences," *Ultrasound Med. Biol.*, vol. 44, no. 1, pp. 153–167, Jan. 2018.

[15] J. Dorazil, R. Repp, T. Kropfreiter, R. Prüller, K. Říha, and F. Hlawatsch, "A multitarget tracking method for estimating carotid artery wall motion from ultrasound sequences," in *Proc. EUSIPCO 2019*, A Coruña, Spain, Sep. 2019, pp. 1–5.

[16] S. J. Julier and J. K. Uhlmann, "Unscented filtering and nonlinear estimation," *Proc. IEEE*, vol. 92, no. 3, pp. 401–422, Mar. 2004.

[17] J.-Y. Bouguet, "Pyramidal implementation of the Lucas Kanade feature tracker," Tech. Rep., Intel Corporation, Microprocessor Research Labs, 2000.

[18] J. Dorazil, K. Říha, and M. K. Dutta, "Common carotid artery wall localization in B-mode ultrasound images for initialization of artery wall tracking methods," in *Proc. TSP 2019*, Budapest, Hungary, Jul. 2019, pp. 605–608.

[19] C. Harris and M. Stephens, "A combined corner and edge detector," in *Proc. Alvey Vision Conf.*, Manchester, UK, 1988, pp. 147–152.

[20] S. Kim, A. S. Paul, E. A. Wan, and J. McNames, "Multiharmonic tracking using sigma-point Kalman filter," in *Proc. Ann. Int. Conf. IEEE Eng. Med. Biol. Soc.*, Vancouver, BC, Canada, Aug. 2008, pp. 2648–2652.

[21] W. Nichols, M. O'Rourke, and C. Vlachopoulos, *McDonald's Blood Flow in Arteries: Theoretical, Experimental and Clinical Principles*, London, UK: CRC Press, 6th edition, 2011.

[22] M. Schlaikjer, S. T. Petersen, J. Jensen, and P. Stetson, "Tissue motion in blood velocity estimation and its simulation," in *Proc. IEEE Int. Ultrason. Symp.*, Sendai, Miyagi, Japan, Oct. 1998, pp. 1495–1499.

[23] S. Challa, M. R. Morelande, D. Mušicki, and R. J. Evans, *Fundamentals of Object Tracking*, Cambridge, UK: Cambridge University Press, 2011.

[24] J. Stoitsis, S. Golemati, E. Bastouni, and K. S. Nikita, "A mathematical model of the mechanical deformation of the carotid artery wall and its application to clinical data," in *Proc. Ann. Int. Conf. IEEE Eng. Med. Biol. Soc.*, Lyon, France, Aug. 2007, pp. 2163–2166.

[25] J. A. Jensen, "Field: A program for simulating ultrasound systems," in *Proc. Nordic-Baltic Conf. Biomed. Eng.*, Tampere, Finland, Jun. 1996, pp. 351–353.

[26] J.-Y. Bouguet, "Pyramidal implementation of the affine Lucas Kanade feature tracker: Description of the algorithm," Tech. Rep., Intel Corporation, Microprocessor Research Labs, 2001.